Published by IOP Publishing for Sissa Medialab

Received: *November 3, 2024*
Accepted: *January 23, 2025*
Published: *February 18, 2025*

Topical Workshop on Electronics for Particle Physics
University of Glasgow, Scotland, U.K.
30 September–4 October 2024

# Evaluation of efficiency, radiation hardness, and timing performance of the Analogue Pixel Test Structure for ALICE ITS3

**J. Liu on behalf of the ALICE collaboration**

*Department of Physics, University of Liverpool,*
*Oxford Street, Liverpool, U.K.*

*E-mail:* j.l.liu@liverpool.ac.uk

Abstract: A replacement of the three innermost layers of the new ALICE Inner Tracking System (ITS2), referred to as ITS3, is planned for the LHC Long Shutdown 3 (2026–2028) to further enhance tracking precision and efficiency. The ITS3 is designed as a cylindrically bent silicon vertex detector, utilizing stitched, wafer-scale sensors developed with the Tower Partners Semiconductor Co. 65 nm technology. The feasibility of this technology for ITS3 was evaluated using prototypes fabricated in the initial multi-reticle-layer run. This contribution presents the latest sensor characterization results from the analogue pixel test structures, focusing on detection efficiency, timing response, and radiation hardness.

Keywords: Particle tracking detectors; Solid state detectors; Radiation-hard detectors; Timing detectors



https://doi.org/10.1088/1748-0221/20/02/C02037

2025 JINST 20 C02037

## Contents



## 1 Introduction

The upgraded Inner Tracking System (ITS2) [1, 2] of the ALICE experiment at the LHC, featuring CMOS monolithic active pixel sensors (MAPS), known as ALPIDE [3], is currently operational and demonstrating excellent performance in LHC Run 3. The forthcoming ITS3 [4, 5], scheduled for installation during the LHC Long Shutdown 3 (2026–2028), aims to enhance tracking precision and efficiency. The impact-parameter resolution is expected to improve by a factor of two compared to ITS2, up to transverse momenta of about 5 GeV/$c$. Additionally, simulations show that the track-reconstruction efficiency of ITS3 will remain above 90% down to 100 MeV/$c$ and 60% down to 60 MeV/$c$, offering up to a 30% gain over ITS2. ITS3 will feature a cylindrically curved silicon vertex detector based on stitched, wafer-scale MAPS developed using the 65 nm process technology from Tower Partners Semiconductor Co. (TPSCo) [6].

The initial assessment of this technology dates back to 2021, through the first multi-layer reticle submission, which includes test structures such as the Analogue Pixel Test Structure (APTS). The APTS architectures are briefly described in section 2. The latest sensor characterization results from both laboratory measurements and test beams are discussed in section 3.

## 2 The Analogue Pixel Test Structure

The APTS, featuring a $6 \times 6$ pixel matrix with direct analogue readout for the central $4 \times 4$ pixels, was designed with two output buffer variants positioned at the periphery of the pixel matrix: a source-follower (APTS-SF) and a fast operational amplifier (APTS-OA). Both variants share the same in-pixel circuit, where the low input capacitance stage consists of two source followers that buffer the input signal from the sensor. The basic source follower structure in APTS-SF provides a reliable analogue readout but operates at a slower speed, whereas the high-speed operational amplifier in APTS-OA enables the study of intrinsic time resolution. Sensor variants included different pixel pitches ranging from 10 µm to 25 µm, with variations in the geometry and size of the p-well and n-well collection electrodes, fabricated using three processes: standard, modified, and modified-with-gap.

In comparison to the standard process, the modified process incorporates a deep low-dose n-type implant beneath the entire pixel area, forming a deep planar junction in the sensor. For the modified-with-



2025 JINST 20 C02037

gap process, a 2.5 µm gap is introduced in the low-dose n-type implant at the pixel boundaries, resulting in a vertical junction that enhances the lateral electric field, directing the charge from the pixel boundary towards the collection electrode. Additionally, to study the impact on capacitance and charge collection, the geometry and size of both the n-well collection electrode and the p-well were implemented in four different variants: reference, smaller p-well enclosure, larger n-well collection electrode, and finger-shaped p-well enclosure. Further details on the process and sensor geometries can be found in [7, 8].

The power consumption is primarily determined by the current biases of the front-end circuit and the output buffer. The estimated power consumption per pixel is 6 µW in-pixel and 420 µW in the periphery for APTS-SF, and 150 µW in-pixel and 3.1 mW in the periphery for APTS-OA. The APTS is designed for sensor characterization, while the more realistic front-end circuit for ITS3 has been implemented and characterized using the digital pixel test structure [9]. The APTS supports reverse substrate voltages ($V_{\text{sub}}$) within the range of 0 to −5 V.

## 3 Sensor characterisation

To evaluate the performance of the APTS sensors, a comprehensive set of measurements was conducted, focusing on energy calibration, charge distribution, detection efficiency, radiation tolerance, in-pixel efficiency, and intrinsic timing resolution. The following subsections provide detailed findings on each of these performance aspects.

### 3.1 Energy calibration

Measurements using the $^{55}$Fe source were performed to evaluate the chip's charge collection and energy resolution across various design variants with multiple pixel pitches. Figure 1(a) shows a representative spectrum for the seed signal of events with a cluster size equal to unity, measured using the APTS-SF modified-with-gap design. A cluster is defined as a 3×3 matrix centered on the pixel with the highest amplitude (the seed), which exceeds a set threshold. The energy resolution is calculated as the full width at half maximum of the Mn-K$_\alpha$ peak (fitted with Gaussian functions) divided by its mean. An energy resolution of 4% was obtained for the modified-with-gap design. A linear relationship between the seed signal and photon energy was established, constrained to pass through the origin, as illustrated in figure 1(b).

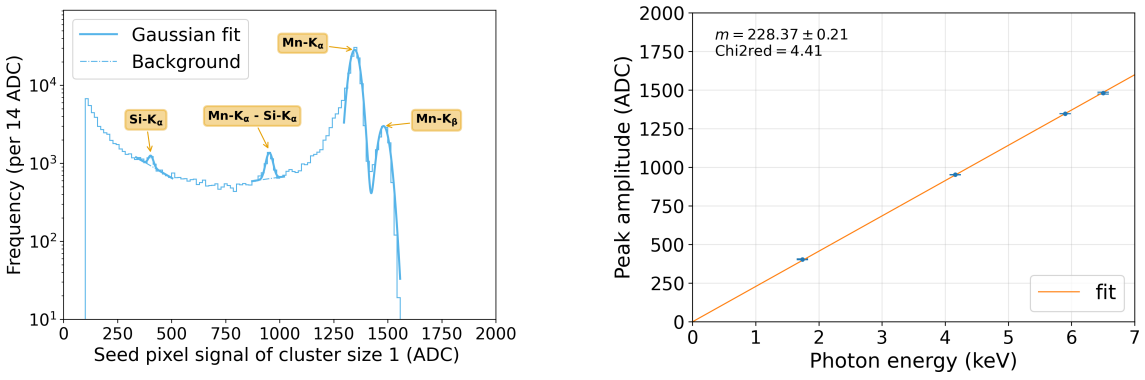


(a) (b)

**Figure 1.** (a) $^{55}$Fe spectrum for events with a cluster size equal to unity. (b) Energy calibration based on peak amplitude estimated as the mean from the Gaussian fit shown in (a), fitted with a linear function. Results are shown for APTS-SF with 15 µm pitch, modified-with-gap, reference variant, $V_{\text{sub}} = -1.2$ V.



2025 JINST 20 C02037

### 3.2 Charge distribution and detection efficiency

Detailed measurements were performed using a 120 GeV/$c$ positive hadron beam at the CERN SPS test beam facility. These measurements evaluated sensor charge collection behavior and detection efficiency under varying conditions, including pixel pitches, sensor designs, and reverse substrate voltages.

Figure 2(a) shows the seed pixel signal distributions for the three APTS-SF designs. A progression from the standard design to the modified and modified-with-gap versions shows an increase in the most probable value (MPV) of the seed signal, enhancing the signal-to-noise ratio by a factor of two. This trend aligns with the reduced charge sharing observed in the $^{55}$Fe measurements. With an MPV of approximately 500 electrons for the modified-with-gap design, the epitaxial thickness is estimated to be around 10 µm. The seed pixel signal distribution was also analyzed for various pixel pitches of APTS-SF with modified-with-gap design, as depicted in figure 2(b). For comparison, measurements using a different setup with the Caribou readout system [10] at the DESY facility, with a 4 GeV/$c$ electron beam, are included. The results from both setups are in good agreement. The MPV slightly increases with larger pitches, which correlates with the reduction in average cluster size observed in the $^{55}$Fe measurements.

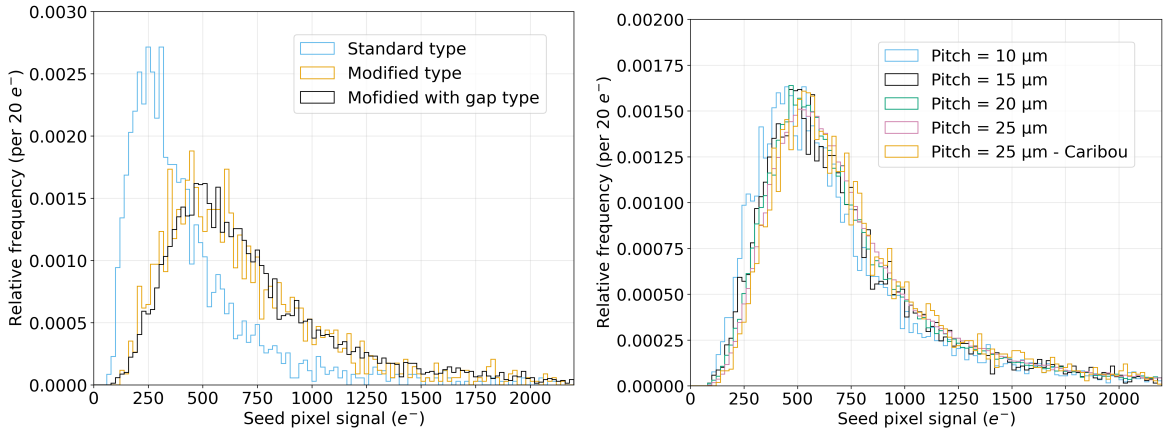


(a) (b)

**Figure 2.** Seed pixel signal charge distribution comparison. (a) Different designs with a 15 µm pitch. (b) Various pixel pitches for modified-with-gap design. Results are shown for APTS-SF with reference variant, at $V_{\text{sub}} = -1.2$ V.

The detection efficiency for different pixel pitches of the APTS-SF with modified-with-gap design at $V_{\text{sub}} = 0$ V, is shown in figure 3, for threshold values greater than three times the noise root mean square (RMS). A detection efficiency of 99% or higher is achieved for all pitches across wide threshold ranges.

### 3.3 Radiation tolerance

The APTS-SF sensors were irradiated using neutron beams and X-ray irradiation systems to carefully investigate the effects of non-ionizing energy loss (NIEL) and total ionizing dose (TID) on sensor performance. An efficiency of $\geq 99\%$ was achieved for all pitches of the modified-with-gap design up to a NIEL of $10^{14}$ 1 MeV $n_{eq}$ cm$^{-2}$, while maintaining a wide operational threshold range. Notably, for the 15 µm pitch, this efficiency level was maintained up to a NIEL of $1 \times 10^{15}$ 1 MeV $n_{eq}$ cm$^{-2}$, as



2025 JINST 20 C02037

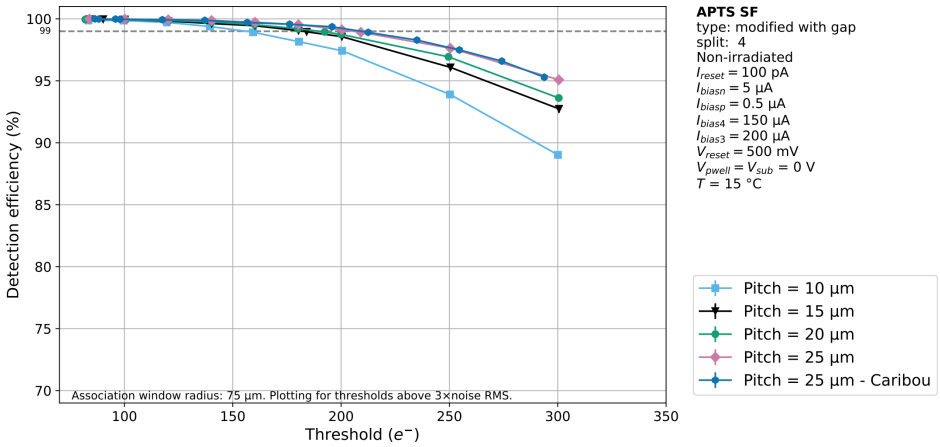


**Figure 3.** Efficiency comparison between different pixel pitches. Results are shown for APTS-SF with modified-with-gap design, reference variant, at $V_{\text{sub}} = 0$ V and 15°C.

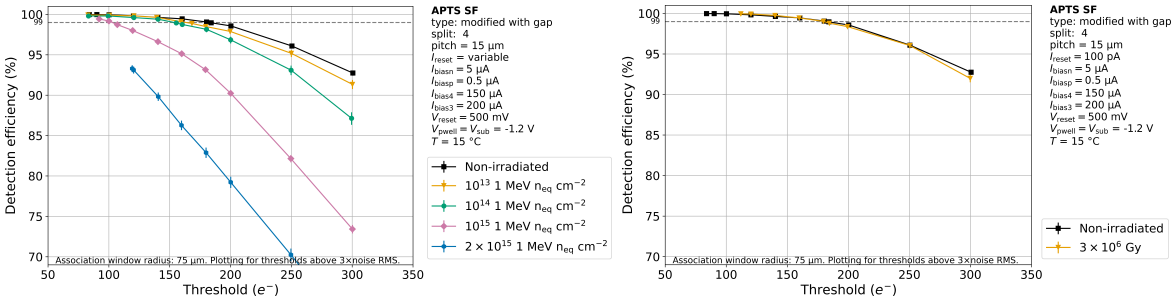


(a) (b)

**Figure 4.** (a) Efficiency comparison for a non-irradiated sensor and sensors exposed to different NIEL levels. (b) Efficiency comparison between a non-irradiated sensor and one exposed to a TID of $3 \times 10^6$ Gy. Results are shown for the APTS-SF with 15 µm pitch, modified-with-gap, reference variant, at $V_{\text{sub}} = -1.2$ V and 15°C.

illustrated in figure 4(a). This performance exceeds the ITS3 requirement of $10^{13}$ 1 MeV $n_{eq}$ $cm^{-2}$. As shown in figure 4(b), after exposure to $3 \times 10^6$ Gy, the detection efficiency remained above 99% across a wide threshold range, meeting the TID requirements for ITS3. It also fulfils the requirements for the proposed ALICE 3 [11] vertex detector, a project supposed to be operational during LHC Run 5 to extend tracking and vertexing capabilities beyond those of ITS3.

### 3.4 In-pixel efficiency

To investigate the source of detection efficiency loss, the dependence on the particle hit location within a pixel was analyzed. Figure 5 shows the detection efficiency of the reference variant pixel geometry of a non-irradiated APTS-SF with modified-with-gap design as a function of the reconstructed track position relative to the nearest pixel center. As expected, the detection efficiency decreases as the particle track moves farther from the collection diode. Similar trends were observed across other pixel geometry variations.



2025 JINST 20 C02037

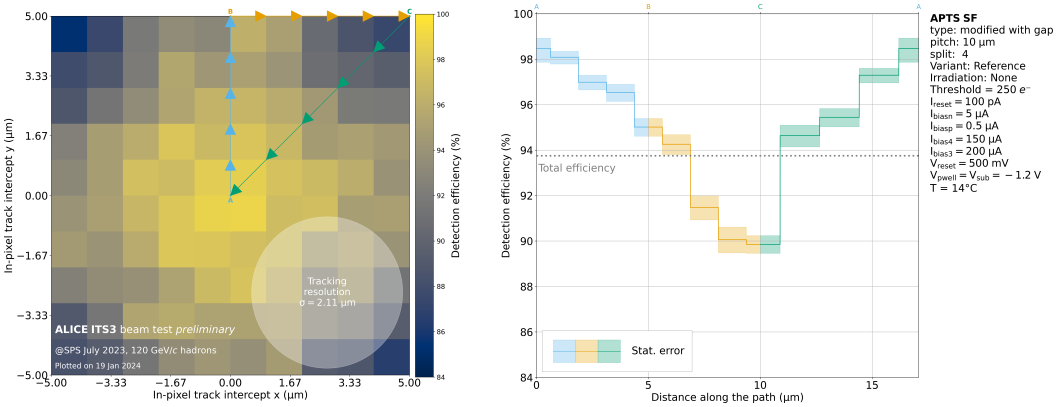


**Figure 5.** In-pixel detection efficiency map (left) and efficiency along specific routes (right), with routes indicated by matching colors in the left panel. The tracking resolution is shown as a white circle ($r = \sigma_{\text{track}} = 2.11$ µm). Results are for the APTS-SF with 10 µm pitch, modified-with-gap, reference variant, at $V_{\text{sub}} = -1.2$ V and 14°C.

### 3.5 Intrinsic time resolution

The intrinsic timing performance of this new technology was assessed using the APTS-OA. A low gain avalanche detector (LGAD) was installed alongside the test beam telescope as a timing reference plane. Figure 6 shows the time residual distribution for the modified-with-gap design with a 10 µm pitch. The time resolution of the APTS-OA was determined by using $\text{RMS}_{99.7\%}$ as the width of the time residual distribution. After accounting for the time resolution of the LGAD (30 ps), the intrinsic time resolution of the APTS-OA is approximately 63 ps.

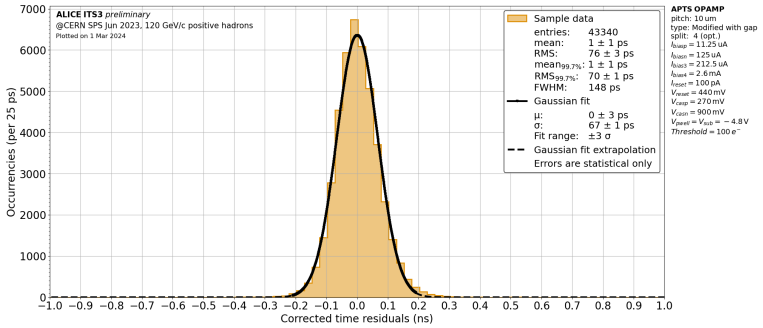


**Figure 6.** Time residuals measured for the APTS-OA with 10 µm pitch, modified-with-gap, reference variant, at $V_{\text{sub}} = -4.8$ V.

The uniformity of timing performance across the pixel surface was examined by analyzing the relationship between time resolution and in-pixel track position. Figure 7 illustrates the variation in time resolution as a function of the radial distance of the reconstructed hit from the pixel center. As anticipated, the optimal time resolution of about 52 ps was achieved at the pixel center, where the proximity to the collection electrode is greatest, resulting in the highest electric field strength.

## 4 Conclusion

Extensive measurements and analyses were carried out to evaluate the performance of the APTS under various conditions, including different pixel designs and radiation exposures. The APTS has



2025 JINST 20 C02037

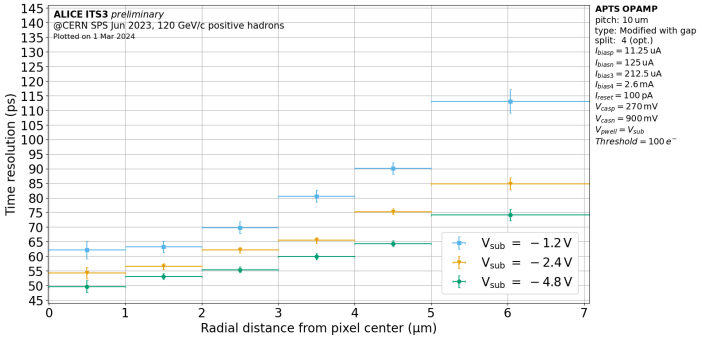


**Figure 7.** Time resolution as a function of the radial distance of the reconstructed hit from the pixel center for the APTS-OA with 10 µm pitch, modified-with-gap, reference variant.

demonstrated promising performance in terms of detection efficiency, radiation hardness, and timing resolution, meeting the requirements for the ALICE ITS3 upgrade. The modified-with-gap design showed significant improvements in charge collection and radiation tolerance, while the APTS-OA achieved an intrinsic time resolution of 63 ps. These results confirm the feasibility of employing 65 nm TPSCo technology for future upgrades of the ALICE experiment, providing a robust basis for enhanced tracking capabilities in LHC Run 4 and beyond.

## References


[1] ALICE collaboration, *Technical Design Report for the Upgrade of the ALICE Inner Tracking System*, *J. Phys. G* **41** (2014) 087002.

[2] ALICE collaboration, *ALICE upgrades during the LHC Long Shutdown 2*, 2024 *JINST* **19** P05062 [arXiv:2302.01238].

[3] G.A. Rinella, *The ALPIDE pixel sensor chip for the upgrade of the ALICE Inner Tracking System*, *Nucl. Instrum. Meth. A* **845** (2017) 583.

[4] ALICE collaboration, *Technical Design report for the ALICE Inner Tracking System 3 — ITS3; A bent wafer-scale monolithic pixel detector*, CERN-LHCC-2024-003, CERN, Geneva (2024).

[5] J. Liu, *ALICE ITS3: A truly cylindrical vertex detector based on bent, wafer-scale stitched CMOS sensors*, *Nucl. Instrum. Meth. A* **1064** (2024) 169355.

[6] Tower Partners Semiconductor Co, Last accessed 25 October 2024, http://www.towersemi.com/.

[7] G.A. Rinella et al., *Characterization of analogue Monolithic Active Pixel Sensor test structures implemented in a 65 nm CMOS imaging process*, *Nucl. Instrum. Meth. A* **1069** (2024) 169896 [arXiv:2403.08952].

[8] G.A. Rinella et al., *Time performance of Analog Pixel Test Structures with in-chip operational amplifier implemented in 65 nm CMOS imaging process*, *Nucl. Instrum. Meth. A* **1070** (2025) 170034 [arXiv:2407.18528].

[9] G.A. Rinella et al., *Digital pixel test structures implemented in a 65 nm CMOS process*, *Nucl. Instrum. Meth. A* **1056** (2023) 168589 [arXiv:2212.08621].

[10] T. Vanat, *Caribou — A versatile data acquisition system*, *PoS* **TWEPP2019** (2020) 100.

[11] ALICE collaboration, *Letter of intent for ALICE 3: A next generation heavy-ion experiment at the LHC*, arXiv:2211.02491 [CERN-LHCC-2022-009].




2025 JINST 20 C02037